Fluorination of Epitaxial Oxides: Synthesis of Perovskite Oxyfluoride Thin Films

ARTICLE *in* JOURNAL OF THE AMERICAN CHEMICAL SOCIETY · JANUARY 2014

Impact Factor: 12.11 · DOI: 10.1021/ja410954z · Source: PubMed

6 AUTHORS, INCLUDING:

Eun Ju Moon
Drexel University
48 PUBLICATIONS **198** CITATIONS
SEE PROFILE

Eric D. Laird
Drexel University
18 PUBLICATIONS **175** CITATIONS
SEE PROFILE

Christopher Y Li
Drexel University
93 PUBLICATIONS **2,986** CITATIONS
SEE PROFILE

Steven J. May
Drexel University
62 PUBLICATIONS **1,125** CITATIONS
SEE PROFILE

JACS
JOURNAL OF THE AMERICAN CHEMICAL SOCIETY
Communication
pubs.acs.org/JACS

Fluorination of Epitaxial Oxides: Synthesis of Perovskite Oxyfluoride Thin Films

Eun Ju Moon,*[,†] Yujun Xie,[†] Eric D. Laird,[†] David J. Keavney,[‡] Christopher Y. Li,[†] and Steven J. May*[,†]

[†]Department of Materials Science and Engineering, Drexel University, Philadelphia, Pennsylvania 19104, United States
[‡]X-ray Sciences Division, Advanced Photon Source, Argonne National Laboratory, Argonne, Illinois 60439, United States

Supporting Information

ABSTRACT: While the synthesis of ABO_3 perovskite films has enabled new strategies to control the functionality of this material class, the chemistries that have been realized in thin film form constitute only a fraction of those accessible to bulk chemists. Here, we report the synthesis of oxyfluoride films, where the incorporation of F may provide a new means to tune physical properties in thin films by modifying electronic structure. Fluorination is achieved by spin coating a poly(vinylidene fluoride) (PVDF) solution onto oxygen-deficient films. The film/polymer bilayer is then annealed, promoting the diffusion of F into the film. We have used this method to synthesize $SrFeO_{3-\alpha}F_{\gamma}$ films, as confirmed by X-ray photoemission spectroscopy and X-ray absorption spectroscopy.

Advances in thin film deposition techniques[1,2] have enabled the synthesis of perovskite films and superlattices with monolayer precision and abrupt interfaces between dissimilar compounds. The realization of high-quality films has enabled new strategies, such as biaxial epitaxial strain[3−6] and the stabilization of metastable cation-ordered superlattices,[7−10] with which to control and enhance functional properties in oxides. Despite the great strides made in oxide film deposition, a number of limitations remain, foremost of which is the restricted range of chemistries afforded in film deposition. In particular, film-based perovskite research has been restrained to compounds with oxygen on the anion site, in part due to contamination concerns associated with introducing gases such as fluorine or chlorine into expensive vacuum chambers used for oxide deposition. However, oxyfluorides and other mixed anion perovskites exhibit an array of functional properties including superconductivity,[11] ionic conductivity,[12] and robust magnetic behavior[13] that may yield new applications or insights into fundamental structure−property relations when studied in thin film form. Furthermore, the substitution of F for O on the anion site provides an appealing alternative to oxygen vacancies as a means to electron dope perovskites, a capability necessary for the realization of diverse and multifunctional oxide electronics.[14] For example in bulk, conversion of $SrFeO_3$ to $SrFeO_2F$ has been shown to reduce the Fe oxidation state,[15] while studies of $La_{1-x}Sr_xFeO_3$ fluorination to $La_{1-x}Sr_xFeO_{3-x}F_x$ have demonstrated changes in atomic structure[16] and magnetic properties.[17] Alternatively, if starting from oxygen-deficient $SrFeO_{2.5}$, fluorine insertion into the vacant anion sites (yielding $SrFeO_{2.5}F_{0.5}$) would be expected to increase the Fe oxidation state.

We report the synthesis of $SrFeO_{3-\alpha}F_{\gamma}$ oxyfluoride thin films via the coannealing of as-grown oxygen-deficient films with a fluorine containing polymer, a process adapted from previous work on bulk polycrystals.[15,16,18,19] The presence of fluorine throughout the thickness of the films was confirmed using X-ray photoemission spectroscopy (XPS), while X-ray diffraction (XRD), X-ray absorption spectroscopy (XAS), and temperature-dependent resistivity were used to investigate fluorine induced changes to the structural and electronic properties of the films. This work demonstrates a straightforward and widely accessible route to stabilizing epitaxial mixed-anion perovskite films and heterostructures.

Oxygen-deficient $SrFeO_{3-\delta}$ thin films were grown with oxide molecule beam epitaxy on $SrTiO_3$ (STO) substrates. During deposition, the substrate temperature was held at ∼600 °C, and O_2 was sourced to the substrate at a rate that yielded a chamber pressure of $\sim 2 \times 10^{-6}$ Torr. These conditions were chosen to yield highly oxygen-deficient $SrFeO_{3-\delta}$. Growth was monitored by *in situ* reflection high-energy electron diffraction (RHEED). The atomic fluxes for the cation deposition were calibrated using Rutherford backscattering spectroscopy. The thickness of the films was ∼23 nm (60 unit cells). Following fluorination, which is described below, multiple characterization techniques were performed. XRD measurements were taken around the (0 0 2) truncation rod of the film, using a Rigaku SmartLab diffractometer equipped with a parabolic mirror and a four bounce/axis monochromator on the incident and diffracted beams. The XPS depth profiling was done on a ThermoFisher K-Alpha spectrometer using monochromated $Al_{K\alpha}$ source, with a pass energy of 20 eV at Rutgers University. For sputter depth profiling, Ar^+ ions of 2 keV energy at a scan size of 2×2 mm^2 and a 60 s sputter interval were used. To minimize effects of charging on the insulating films, a low-energy electron gun was used for charge neutralization. Resonant soft X-ray spectroscopy was performed at the beamline 4-ID-C of the Advanced Photon Source at Argonne National Laboratory in total electron yield mode to probe the O and F K-edges and Fe L_{2-3} edges at 300 K.

Fluorination of oxygen-deficient $SrFeO_{3-\delta}$ was performed using a simple two-step procedure: (1) A solution of PVDF (10 wt % in dimethylformamide) was spin coated onto the as-grown $SrFeO_{3-\delta}$ films. Spin coating was done using successive cycles at rotation rates of 500 rpm for 5 s followed by 2000 rpm for 25 s.

Received: November 1, 2013

   dx.doi.org/10.1021/ja410954z | J. Am. Chem. Soc. XXXX, XXX, XXX−XXX

The coated PVDF was dried overnight in an ambient environment. (2) The bilayer was heated, and the polymer was thermally decomposed in a horizontal quartz tube under a slow O_2 flow at 600 °C for 2 h.[20] The possible reaction equation is shown in the bottom of Scheme 1, in which carbon and hydrogen form CO_2 and H_2O, respectively, as byproducts along with some PVDF oligomers.[21] In this scenario, the flow of oxygen helps to mitigate carbon contamination in the film from the decomposing PVDF. Additionally, previous work has shown that carbon, decomposed from the polymer, can act to reduce the metal oxide.[24] This would decrease the oxygen content in the film, potentially enabling a larger concentration of fluorine than the initial oxygen vacancy concentration in the as-grown film.[25] At the completion of the reaction, fluorine atoms occupy anion (oxygen) sites yielding $SrFeO_{3-\alpha}F_\gamma$ (SFO-F, hereafter), which is illustrated in the upper right panel of Scheme 1.

Figure 1 shows XRD measurements taken around the pseudocubic (0 0 2) truncation rod of a strontium ferrite thin

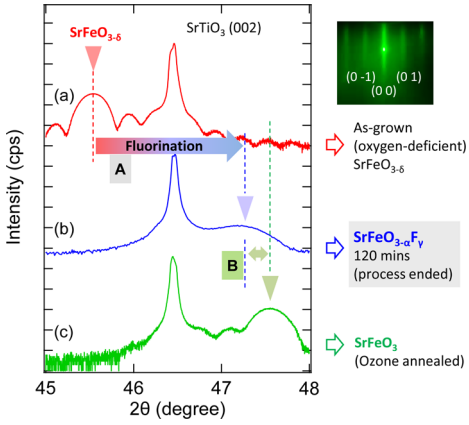

Figure 1. XRD data of SFO before and after fluorination process. (a) Oxygen-deficient SFO (inset: RHEED image from as-grown film), (b) fluorinated SFO-F film, and (c) ozone annealed $SrFeO_3$ film (SFO_3). Film (0 0 2) peaks indicated by dashed arrows on SFO, SFO-F, and SFO_3. (A) shows the (0 0 2) peak shift upon fluorinating the as-grown film and (B) shows a difference of *c*-axis lattice parameter of SFO-F and ozone-annealed SFO_3 films.

film before and after the fluorination process, along with the STO (0 0 2) peak. First, the RHEED image of the as-grown film shows well-defined streaks at the (0 1), (0 0), and (0 $\bar{1}$) reflections, confirming the surface quality of the epitaxial $SrFeO_{3-\delta}$ thin film, as shown in inset. The *c*-axis parameter of the as-grown oxygen-deficient $SrFeO_{3-\delta}$ thin film on STO is found to be ~3.979 Å, as shown in (a), which is comparable to previous reports of Brownmillerite $SrFeO_{2.5}$ films grown on STO.[26] This suggests that the oxygen deficiency in the as-grown film is close to $\delta \sim 0.5$. While short annealing (10 min) of the polymer/film bilayer does not result in a clear diffraction peak from the film, after completion of a 2 h anneal, the XRD data reveal the presence of a Bragg peak indicating a contraction of the *c*-axis parameter to 3.848 Å in the SFO-F film (Figure 1b). The (0 0 2) peak of the SFO-F film is broadened and exhibits a weaker intensity compared to the as-grown film, indicating a degradation of crystalline quality compared to SFO. It is anticipated that further refinements of the processing conditions will lead to improved crystalline quality.

To compare between films in perovskite heterostructures with fully occupied anion sites, a nominally oxygen stoichiometric

Scheme 1. Schematics of the Fluorination Process Carried out on a Bilayer Consisting PVDF and an Oxygen-Deficient $SrFeO_{3-\delta}$ Thin Film[a]

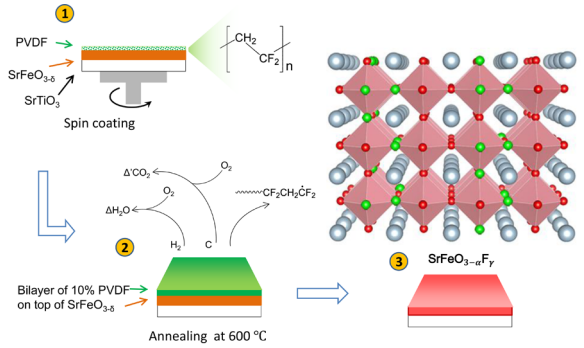

$$SrFeO_{3-\delta} + 0.1\,[CH_2{-}CF_2]_n \rightarrow SrFeO_{3-\alpha}F_\gamma + \Delta H_2O\uparrow + \Delta' CO_2\uparrow + \sim\!\sim CF_2CH_2\dot{C}F_2$$

[a]PVDF (CH_2CF_2) of 10% was spin coated on oxygen-deficient $SrFeO_{3-\delta}$ film grown on STO (1). Heat treatment of fluorination process (2) is illustrated with the possible reaction equation as shown below. After the process, final product, $SrFeO_{3-\alpha}F_\gamma$, is obtained (3). Green and red spheres represent fluorine and oxygen, respectively.

$SrFeO_3$ film, achieved by annealing in an O_3/O_2 mixture at 200 °C after oxygen annealing at 600 °C, was measured. The XRD results are shown in Figure 1c. The *c*-axis lattice parameter of the $SrFeO_3$ is 3.826 Å, indicating that the fluorinated ferrite thin film has a 0.6% *c*-axis expansion compared to $SrFeO_3$ (B). It is noted that cell volume of SFO-F on STO is larger than cell volume of $SrFeO_3$ on STO likely because the atomic radii of Fe^{3+} is larger than Fe^{4+}.[16]

To probe the inward diffusion of the fluorine into the oxygen-deficient $SrFeO_{3-\delta}$, XPS depth profile analysis was performed via ion sputtering of the film after the fluorination process. Figure 2a,b shows the evolution of F 1s and Ti 2p core lines in the XPS depth profile through the fluorinated $SrFeO_{3-\alpha}F_\gamma$ (SFO-F) film to the STO substrate after sputter etching for 11 cycles. The slight shift with the layer depth toward higher energies (see Figure 2a) can be attributed to the compositional gradient of the $FeO_{3-\alpha}F_\gamma$ layer and to the bonding among O−Fe−F. The Ti 2p spectrum is composed of spin−orbit split doublet Ti $2p_{3/2}$ and Ti $2p_{1/2}$ including satellites, which appears after a few cycles of ion sputtering, indicating that the sputtering depth has exceeded that of the film thickness and reached the STO substrate.

The series of XPS spectrum was recorded for the top surface of the film as well as after Ar^+ ion sputtering, and the obtained spectra were the Sr 2p, Fe 2p, Ti 2p, O 1s, and F 1s photoelectron peaks. The left panel of Figure 3c shows a normalized concentration−depth profile for a $SrFeO_{3-\alpha}F_\gamma$ film. It was derived from integrated peak areas, since a quantitative description is complicated due to differences in scattering cross sections and the Ar^+ ion sputter yield of each element in the film and substrate. Carbon contamination was found only at the outermost surface before any sputtering was performed. Following the first sputtering cycle, no carbon peak was detected. The evolution of the Fe 2p and Ti 2p peaks allows for approximate determination of the penetration depth, indicating if the SFO-F or STO layers are being probed. As can be seen in Figure 2c, fluorine is present throughout the SFO layer, indicating that the fluorine atoms have diffused in the oxygen-deficient film. The intensity of the F and Fe peaks decreases at the depth where the Ti intensity begins to appear. With further depth profiling, the F peak is absent within the STO substrate. Additionally, the relative

dx.doi.org/10.1021/ja410954z | J. Am. Chem. Soc. XXXX, XXX, XXX−XXX

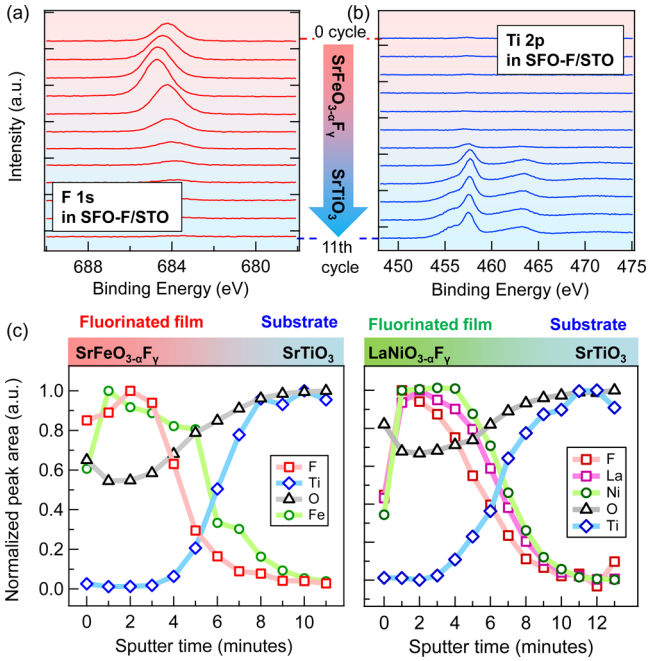

Figure 2. XPS depth profile analysis showing the evolution of (a) F 1s and (b) Ti 2p core lines for different penetration depths of a $SrFeO_{3-\alpha}F_{\gamma}$ (SFO-F) film on a STO substrate. Series of spectra throughout the ion sputtering cycle (total 11 cycles) is displayed from top to bottom. (c) Normalized concentration-depth profile for SFO-F (left) and $LaNiO_{3-\alpha}F_{\gamma}$ (right) on STO film; another fluorinated transition-metal perovskite oxide thin film example.

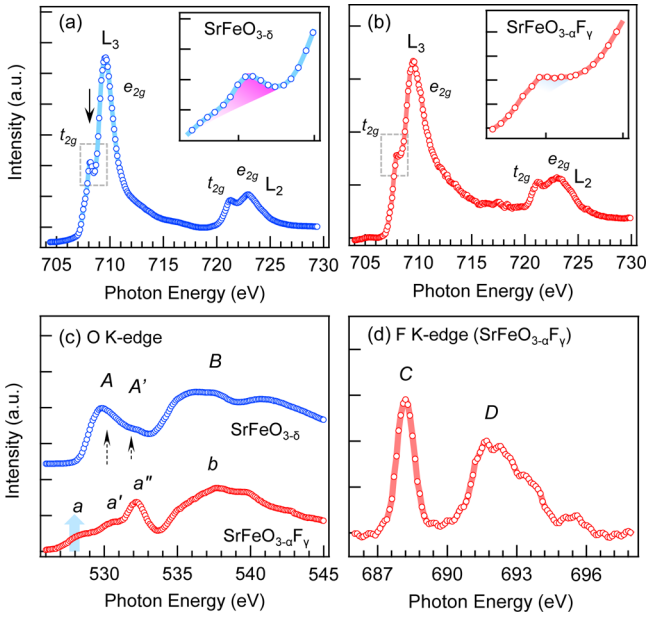

Figure 3. XAS spectra of Fe $L_{2,3}$-edge of (a) oxygen-deficient as-grown $SrFeO_{3-\delta}$ film and (b) fluorinated $SrFeO_{3-\alpha}F_{\gamma}$. Downward arrow shows t_{2g} states. Inset: Enlarged peak of each t_{2g} electron state of L_3 edge. (c) O K-edge of oxygen-deficient (top, blue) and fluorinated (bottom, red) films. Arrows indicate two split orbitals to $t_{2g}\downarrow$ and $e_g\downarrow$ of the deficient film. Blue thick arrow represents appearance of a prepeak near Fermi level. (d) F K-edge of corresponding fluorinated $SrFeO_{3-\alpha}F_{\gamma}$.

oxygen concentration is lower in the film than the substrate, consistent with the intentional oxygen deficiency in the as-grown thin film. Within the SFO-F film, the fluorine concentration shows a relative maximum at the same depth where the oxygen peak is minimized.

The fluorination process was also carried out on a $LaNiO_{3-\delta}$ film grown on STO. As can be seen in the right panel of Figure 2c, XPS measurements confirm that fluorine is incorporated throughout the nickelate film, similar to SFO-F, indicating that the fluorination process is not limited to ferrites but instead can be widely applied to oxygen-deficient perovskite films.

To verify that the fluorination process alters the electronic structure of the film, XAS was performed at the Fe $L_{2,3}$-edge and O and F K-edges, as shown in Figure 3. The Fe L-edge XAS directly probes the electron dipole transition from 2p core level to 3d valence states. The degeneracy of the Fe 2p core hole level is lifted by the spin−orbit coupling, resulting in the $2p_{3/2}$ and $2p_{1/2}$ multiplets (L_3 and L_2, respectively).[27] The octahedral crystal field lifts the degeneracy of the 3d level so that two levels with t_{2g} and e_g symmetry are created, as presented in Figure 3a. Thus, the spectra are sensitive to factors that change 3d orbital splitting and occupation, such as local symmetry, ligand field, and iron valence.[28−30] For example, spectral changes are observed to the overall shape near the t_{2g} orbital (inset of Figure 3a,b), and an increased peak width of the iron L_3-edge is observed in the oxyfluoride SFO-F film compared to an oxygen-deficient SFO. The broadening of the L_3 peak leading to the reduced t_{2g} intensity upon fluorination is attributed to the fluorine-induced change in the nominal iron valence from Fe^{3+} (d_5) to a mixed Fe^{3+}/Fe^{4+} valence, or more accurately a mixed $d_5/d_5\underline{L}$ state (where $\underline{L}$ denotes a ligand hole).[27,30,31] Alternatively, the L_3 broadening could arise from increased structural disorder; however the oxygen spectra, described below, is also consistent with fluorine-induced changes to the electronic structure.

The influence of fluorination on the conduction band states can also be seen in the O K-edge XAS spectra of SFO and SFO-F films, corresponding to transitions into unoccupied 2p states of ligand atoms hybridized with Fe 3d and Sr 4d, as shown in Figure 3c. We observe three structures denoted by *A*, *A′*, and *B* in a SFO thin film (top in blue). The features *A* and *A′* are assigned to a doublet structure of $t_{2g}\downarrow$ and $e_g\downarrow$ orbitals, respectively, associated with the minority spin Fe $3d_5$ band.[30,32] Structure *B* is assigned to hybridized states of Sr 4d and O 2p. In contrast, the fluorinated film exhibits a triplet structure in the Fe 3d-derived states, denoted *a*, *a′*, and *a″*. Due to the presence of the mixed iron valence, some of the majority spin Fe 3d states are unoccupied in the fluorinated film leading to new transitions. Thus, the peaks *a*, *a′*, and *a″* are assigned to oxygen states hybridized with the $e_g\uparrow$, $t_{2g}\downarrow$, and $e_g\downarrow$ Fe 3d bands, respectively. Figure 3d shows the F K-edge XAS spectrum of the fluorinated film. Based on previous XAS assignments of F bonded to Fe, we attribute the peak *C* to the incorporation of F into the FeO_{6-x} octahedral structure.[33,34] The feature *D* is assigned to F−Sr.

The fluorination process also affects electronic transport properties, as can be seen Figure 4. After fluorination, the room-temperature resistivity of the $SrFeO_{3-\alpha}F_{\gamma}$ film is reduced by over 5 orders of magnitude compared to the as-grown $SrFeO_{3-\delta}$ film. The decreased resistivity is consistent with the XAS results demonstrating an increased nominal iron valence attributed to the F anions occupying the oxygen vacancy sites; a similar decrease in resistivity is observed in bulk $(La,Sr)FeO_3$ with increasing Sr cation substitution.[35] For comparison, we also show the resistivity of a nominally oxygen stoichiometry $SrFeO_3$ film. The difference in resistivity between the $SrFeO_{3-\alpha}F_{\gamma}$, $SrFeO_{3-\delta}$, and $SrFeO_3$ films is considerably larger than typical sample to

dx.doi.org/10.1021/ja410954z | J. Am. Chem. Soc. XXXX, XXX, XXX−XXX

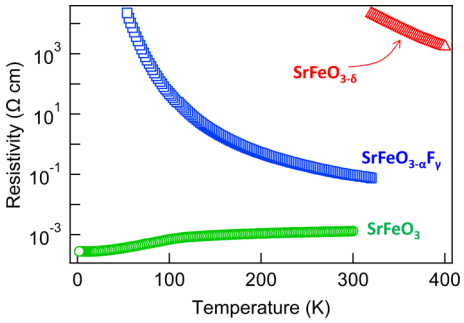

Figure 4. Resistivity as a function of temperature of 60 uc SFO_3 (green), 100 uc SFO-F (blue), and 100 uc SFO (red) thin films.

sample variation for films of the same composition (see Supporting Information).

In conclusion, we have successfully synthesized oxyfluoride perovskite thin films, $SrFeO_{3-\alpha}F_\gamma$, via a reaction with PVDF and demonstrated that the anionic substitution has significant effects on the electronic structure. This partial occupation of fluorine on the oxygen sites potentially enables a new route to controlling the functional properties of complex oxide heterostructures.

■ ASSOCIATED CONTENT

Supporting Information

Resistivity and XPS data. This material is available free of charge via the Internet at http://pubs.acs.org.

■ AUTHOR INFORMATION

Corresponding Authors

em582@drexel.edu

smay@coe.drexel.edu

Notes

The authors declare no competing financial interest.

■ ACKNOWLEDGMENTS

This work is supported by the U.S. Army Research Office under grant no. W911NF-12-1-0132. Acquisition of the PPMS was supported by the U.S. Army Research Office under grant no. W911NF-11-1-0283. Use of the Advanced Photon Source, an Office of Science User Facility operated for the U.S. Department of Energy (DOE) Office of Science by Argonne National Laboratory, was supported by the U.S. DOE under contract no. DEAC02-06CH11357.

■ REFERENCES

(1) Dijkkamp, D.; Venkatesan, T.; Wu, X. D.; Shaheen, S. A.; Jisrawi, N.; Min-Lee, Y. H.; McLean, W. L; Croft, M. *Appl. Phys. Lett.* **1987**, *51*, 619.

(2) Eckstein, J. N.; Bozovic, I.; von Dessonneck, K. E.; Schlom, D. G.; Harris, J. S.; Baumann, S. M. *Appl. Phys. Lett.* **1990**, *57*, 931.

(3) Choi, K. J.; Biegalski, M.; Li, Y. L; Sharan, A.; Schubert, J.; Uecker, R.; Reiche, P.; Chen, Y. B.; Pan, X. Q.; Gopalan, V.; Chen, L. Q.; Schlom, D. G. *Science* **2004**, *306*, 1005.

(4) Zeches, R. J.; Rossell, M. D.; Zhang, J. X.; Hatt, A. J.; He, Q.; Yang, C.-H.; Kumar, A.; Wang, C. H.; Melville, A.; Adamo, C.; Sheng, G.; Chu, Y.-H.; Ihlefeld, J. F.; Erni, R.; Ederer, C.; Gopalan, V.; Chen, L. Q.; Schlom, D. G.; Spaldin, N. A.; Martin, L. W.; Ramesh, R. *Science* **2009**, *326*, 977.

(5) Rata, A. D.; Herklotz, A.; Nenkov, K.; Schultz, L.; Dörr, K. *Phys. Rev. Lett.* **2008**, *100*, 076401.

(6) Moon, E. J.; Rondinelli, J. M.; Prasai, N.; Gray, B. A.; Kareev, M.; Chakhalian, J.; Cohn, J. L. *Phys. Rev. B* **2012**, *85*, 121106(R).

(7) Ohtomo, A.; Muller, D. A.; Grazul, J. L.; Hwang, H. Y. *Nature* **2002**, *419*, 378.

(8) Warusawithana, M. P.; Colla, E. V.; Eckstein, J. N.; Weissman, M. B. *Phys. Rev. Lett.* **2003**, *90*, 036802.

(9) Bousquet, E.; Dawber, M.; Stucki, N.; Lichtensteiger, C.; Hermet, P.; Gariglio, S.; Triscone, J.-M.; Ghosez, P. *Nature* **2008**, *452*, 732.

(10) May, S. J.; Ryan, P. J.; Robertson, J. L.; Kim, J.-W.; Santos, T. S.; Karapetrova, E.; Zarestky, J. L.; Zhai, X.; te Velthuis, S. G. E.; Eckstein, J. N; Bader, S. D.; Bhattacharya, A. *Nat. Mater.* **2009**, *8*, 892.

(11) Al-Mamouri, M.; Edwards, P. P.; Greaves, C.; Slaski, M. *Nature* **1994**, *369*, 382.

(12) Sturza, M.; Daviero-Minaud, S.; Kabbour, H.; Gardoll, O.; Mentre, O. *Chem. Mater.* **2010**, *22*, 6726.

(13) Sturza, M.; Kabbour, H.; Daviero-Minaud, S.; Filimonov, D.; Pokholok, K.; Tiercelin, N.; Porcher, F.; Aldon, L.; Mentre, O. *J. Am. Chem. Soc.* **2011**, *133*, 10901.

(14) Ramesh, R.; Schlom, D. G. *MRS Bull.* **2008**, *33*, 1006.

(15) Berry, F. J.; Ren, X.; Heap, R.; Slater, P.; Thomas, M. F. *Solid State Commun.* **2005**, *134*, 621.

(16) Clemens, O.; Kuhn, M.; Haberkorn, R. *J. Solid State Chem.* **2011**, *184*, 2870.

(17) Clemens, O.; Berry, F. J.; Wright, A. J.; Knight, K. S.; Perez-Mato, J. M.; Igartua, J. M.; Slater, P. R. *J. Solid State Chem.* **2013**, *206*, 158.

(18) Kobayashi, Y.; Tian, M.; Eguchi, M.; Mallouk, T. E. *J. Am. Chem. Soc.* **2009**, *131*, 9849.

(19) Hirai, D.; Climent-Pascual, E.; Cava, R. J. *Phys. Rev. B* **2011**, *84*, 174519.

(20) The fluorination process was also attempted using flowing N_2 at 400 and 600 °C instead of O_2. However, under these conditions the PVDF layer was not fully decomposed, leaving a residual coating on the SFO film. Additionally, films that underwent a N_2-based anneal did not exhibit diffraction peaks.

(21) A probable side reaction of fluorination is the creation of hydrofluoric acid (HF), a known PVDF degradation product.[22,23] This mechanism would occur in addition to the pathway shown in Scheme 2 of ref 23.

(22) Zulfiqar, S.; Zulfiqar, M.; Rizvi, M.; Munirt, A.; McNeili, I. C. *Polym. Degrad. Stab.* **1994**, *43*, 423.

(23) Brandrup, J.; Immergut, E. H.; Grulke, E. A.; Abe, A.; Bloch, D. R. *Polymer Handbook*, 4th ed.; John Wiley & Sons: Hoboken, NJ, 2005.

(24) Tsujimoto, Y.; Yamaura, K.; Hayashi, N.; Kodama, K.; Igawa, N.; Matsushita, Y.; Katsuya, Y.; Shirako, Y.; Akaogi, M.; Takayama-Muromachi, E. *Chem. Mater.* **2011**, *23*, 3652.

(25) Due to the uncertainty in the oxygen content before and after the fluorination process, we denote the as-grown oxygen composition as $3-\delta$ and the postfluorination composition as $3-\alpha$.

(26) Yamada, H.; Kawasaki, M.; Tokura, Y. *Appl. Phys. Lett.* **2002**, *80*, 622.

(27) de Groot, F. M. F.; Kotani, A. *Multiplet Core Level Spectroscopy of Solids*; Taylor & Francis: London, 2007.

(28) Cramer, S. P.; de Groot, F. M. F.; Ma, Y.; Chen, C. T.; Sette, F.; Kipke, C. A.; Eichhorn, D. M.; Chan, M. K.; Armstrong, W. H. *J. Am. Chem. Soc.* **1991**, *113*, 7937.

(29) Soriano, L.; Abbate, M.; Vogel, J.; Fuggle, J. C.; Fernández, A.; González-Elipe, A. R.; Sacchi, M.; Sanz, J. M. *Surf. Sci.* **1993**, *290*, 427.

(30) de Groot, F. M. F. *Coord. Chem. Rev.* **2005**, *249*, 31.

(31) Wu, Z. Y.; Benfatto, M.; Pedio, M.; Cimino, R.; Mobilio, S.; Barman, S. R.; Maiti, K.; Sarma, D. D. *Phys. Rev. B* **1997**, *56*, 2228.

(32) Chikamatsua, A.; Matsuyamaa, T.; Hirosea, Y.; Kumigashirac, H.; Oshimac, M.; Hasegawa, T. *J. Electron Spectrosc. Relat. Phenom.* **2012**, *184*, 547.

(33) Vinogradov, A. S.; Fedoseenko, S. I.; Krasnikov, S. A.; Preobrajenski, A. B.; Sivkov, V. N.; Vyalikh, D. V.; Molodtsov, S. L.; Adamchuk, V. K.; Laubschat, C.; Kaindl, G. *Phys. Rev. B* **2004**, *71*, 045127.

(34) Krasnikov, S. A.; Vinogradov, A. S.; Preobrajenski, A. B.; Gridneva, L. K.; Molodtsov, S. L.; Laubschat, C.; Szargan, R. *Phys. Scr.* **2005**, *T115*, 1074.

(35) Maeder, T.; Bednorz, J. G. *J. Eur. Ceram. Soc.* **1999**, *19*, 1507.